



Effects of False-Ceiling on Critical Ventilation Velocity and Maximum Gas Temperature in Tunnel Fires

H. Savalanpour, B. Farhanieh and H. Afshin[†]

Department of Mechanical Engineering, Center of Excellence in Energy Conversion Sharif University of Technology, Tehran, Iran

[†]Corresponding Author Email: Afshin@sharif.edu

(Received January 24, 2020; accepted July 26, 2020)

ABSTRACT

In the present study, the effect of the use of false-ceiling on fire-induced smoke flow characteristics in tunnels is investigated using a 3D developed computational fluid dynamics tool. The critical velocity, the minimum required tunnel ventilation velocity to stop the smoke flow from moving toward the tunnel inlet (toward the upstream of the fire source), and the maximum gas temperature beneath the ceiling are selected to evaluate the smoke flow control in presence of the false-ceiling. The hydraulic height of the cross-sectional geometry of the tunnel is used as the characteristic length in order to dimensional analyze and compare the non-dimensional results. The results indicate that the use of the false-ceiling reduces the critical velocity and the smoke backlayering, while increases the maximum ceiling gas temperature. Reducing the critical velocity results in ventilation cost reduction (positive impact), while increasing the maximum gas temperature beneath the ceiling increases the risk of instrumental and life damages (negative impact). The detailed results and corresponding physical discussions are presented to clarify the reason for the significant differences between the results of the tunnels with and without false-ceiling.

Keywords: Tunnel fire; Smoke control; False-ceiling; ventilation; Fluid dynamics; Computational.

NOMENCLATURE

b_f	fire source length scale	V_c	critical velocity
c_p	specific heat at constant pressure	V_{inlet}	tunnel inlet velocity
g	gravity acceleration	w^*	plume characteristic velocity
\bar{H}	hydraulic height	ρ_∞	air density at ambient temperature
H_{eff}	effective height of the tunnel	ΔT_{max}	the maximum temperature difference between the ceiling gases and ambient
HRR	heat release rate of fire		
HRR_c	convective heat release rate		
LES	large eddy simulation		

1. INTRODUCTION

The critical velocity, the minimum ventilation velocity required to stop the smoke from moving toward the tunnel inlet and to provide a safe fire extinguishing and evacuation, is one of the main factors affecting ventilation energy consumption. In other words, it is important to find the minimum ventilation velocity (critical velocity), in which the smoke backlayering does not occur and the smoke backlayering length (upstream of the fire source) is equal to zero. Also, the maximum temperature of

the fire-induced gases beneath the tunnel ceiling is a critical parameter in fire safety. Therefore, there are various studies investigated the critical velocity, backlayering length of smoke, and maximum gas temperature, by analyzing the corresponding effective parameters, e.g. tunnels geometry, height, cross-sectional shape, and aspect ratio (tunnel width divided by its height). For example, Lou *et al.* investigated the effects of the heat release rates of fire (10, 20, and 30 MW) and exhaust rate (from 0 to 160 m³/h) on the maximum gas temperature in tunnels. They found that the maximum gas

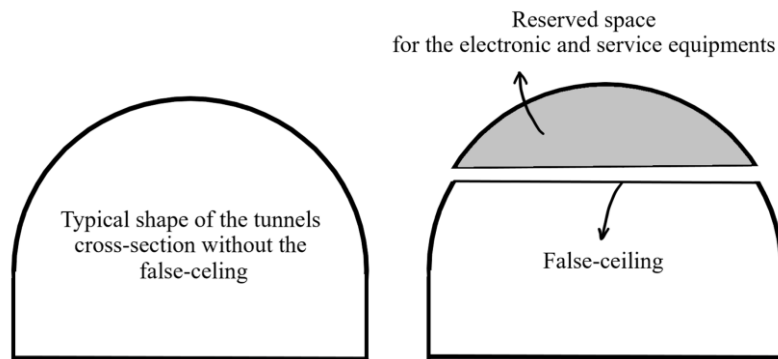


Fig. 1. Practical situation of the false-ceiling.

temperature rise at tunnel vault is proportional to $\frac{3}{4}$ power of non-dimensional heat release rate of fire (Lou *et al.* 2017). Li *et al.* analytically and experimentally investigated the maximum temperature of buoyant gases beneath the tunnel ceiling in presence of fire and found that the heat release rate and the tunnel inlet velocity play important rules in the maximum ceiling gas temperature (Li and Ingason 2012; Li *et al.* 2011). Kazemipour *et al.* simulated the effective parameters on the smoke backlayering such as tunnel cross-sectional aspect ratio, tunnel inlet velocity, tunnel slope, and heat release rate of the fire source in the tunnels (Kazemipour *et al.* 2017; Kazemipour *et al.* 2016). Zhang *et al.* numerically investigated the effects of the turning radius of tunnels on the fire-induced smoke movement in the curved tunnels with turning radiuses of 300-1000 m. They claimed that both the smoke backlayering and the critical velocity increase as the tunnel curvature radius increases and the largest critical velocity corresponds to the straight tunnel with a turning radius of infinity (Zhang *et al.* 2017). Wu and Bakar investigated the critical velocity changes for the different tunnels cross-sectional aspect ratios using the hydraulic height of the tunnel as the characteristic length in the dimensional analysis. They concluded that the tunnel cross-sectional aspect ratio (width/height) plays an important rule in fire-induced smoke flow control (Wu and Bakar 2000). Also, Li and Ingason theoretically and numerically investigated the effects of the cross-sectional aspect ratio. According to the results of Li *et al.* the critical velocity for small fires increases as the tunnel width and height decrease, but it is independent of tunnel width for large fires (Li and Ingason 2017). According to tunnel fire studies in the above literature review, the effects of the use of false-ceiling on fire-induced smoke control were not investigated in the literature, while the false-ceiling is commonly used in the tunnels and changes the tunnels geometry parameters, e.g. tunnel effective flow area and hydraulic height, as shown in Fig.1.

Therefore, in the present study, the effects of the use of false-ceiling in tunnels on fire-induced smoke flow are investigated using a 3D developed computational fluid dynamics tool. The developed method can read any general non-orthogonal grid

using an innovative coordinates transformation method and body-fitted coordinate system. The results of the present study could be used to reduce the critical velocity and the ventilation cost and to improve the tunnel fire safety.

2. DEVELOPED METHOD

2.1 Method Description

A 3D computational fluid dynamics tool is developed here using the non-orthogonal general curvilinear grid to fit well on the curved cross-section of complex geometries such as the investigated tunnels of the present study. The body-fitted grids are mapped to the rectangular spaces using innovative coordinates transformation methods.

The developed method is a far-field fire simulation tool. The far-field methods model the fire as a volumetric heat source (VHS) and do not include combustion in the simulations (Al Hadad *et al.* 2018; Salehi *et al.* 2017; Wang *et al.* 2017). In the present study, the volumetric heat source (VHS) method is used to take into account the effects of the fire presence, in which certain volumetric energy is added to the energy equation (as a source term). The radiation effects of the fire-induced flame are implicated in the calculations using the simple radiation fraction method. By applying the radiation fraction method, a constant fraction of the fire heat release rate is assumed to be lost to the environment without affecting the hot buoyant airflow temperature inside the tunnel. Investigations on different flames proposed that the radiation fraction commonly lies in the range 0.2 to 0.4 (Massachusetts Highway Department/ Federal Highway Administration 1999). Therefore the radiation fraction is set to 0.3 (proposed for propane flames (Ingason *et al.* 2014)) in the present work.

Smagorinsky Large-eddy simulation (LES) model is used to simulate the turbulence effects of the fire-induced smoke flow. The simple implicit grid-filtering is performed by the finite volume discretization. In the Smagorinsky LES model the turbulent viscosity is calculated by the following relation:

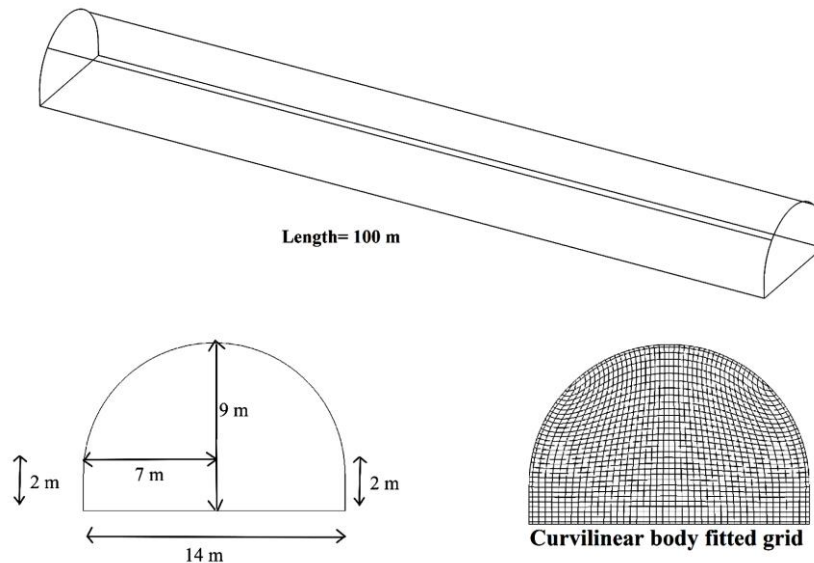


Fig. 2. Geometry and meshing of the investigated tunnel used for the validation.

$$\mu_t = \rho L_s^2 |\bar{S}| \quad (1)$$

where

$$|\bar{S}| = \sqrt{2S_{ij}S_{ij}} \quad (2)$$

In these equations L_s , C_s , S_{ij} and Δ are mixing length, Smagorinsky constant, rate-of-strain tensor, and grid size, respectively. The Smagorinsky coefficient is set to 0.2, which is an appropriate value for the tunnel fire simulations.

The near-wall effects are modeled using the Werner and Wengle (WW) wall function, which is a common model for the tunnel fire simulations (McDermott 2009). WW model is a simplified law of the wall model and proposed by the Werner and Wengle. This model eliminates the sensitivities to grid resolution and also covers all values of y^+ , e.g. the buffer layer ($5 < y^+ < 30$). WW model calculates the non-dimensional tangential velocity as:

$$if(y^+ < 11.81): u^+ = y^+ \quad (3)$$

$$if(y^+ > 11.81): u^+ = 8.3(y^+)^{\frac{1}{7}} \quad (4)$$

The detailed information about the method description and coordinate transformation is presented in our previous study (Savalanpour *et al.* 2019).

2.2 Method Validation

The critical velocity and the maximum temperature of the ceiling gases beneath the ceiling are chosen to validate the developed method. The investigated tunnel geometry used for validation is shown in Fig. 2.

The critical velocity changes due to the changing in HRR calculated by the developed method are

compared with the benchmark data of Li and Ingason., Wu and Bakar, and the experimental results of the real cases of Memorial and Runehamar tunnels (Li and Ingason 2017; Li and Ingason 2018; Massachusetts Highway Department/ Federal Highway Administration 1999; Wu and Bakar 2000). The results have represented in dimensionless form using the hydraulic height of the tunnels as the characteristic length. The dimensional analysis relationships are presented in the equations below, using the hydraulic diameter (\bar{H}) of the tunnel as the characteristic length. The cross-sectional hydraulic heights (four times the flow area divided by the wetted perimeter) of the investigated tunnels without and with the false-ceiling are 10.5m and 9.4m, respectively.

$$\bar{V}_{critical} = \frac{V_{critical}}{\sqrt{g\bar{H}}} \quad (5)$$

$$\overline{HRR} = \left[\frac{HRR}{\rho_\infty T_\infty c_p \sqrt{g\bar{H}^5}} \right] \quad (6)$$

where T_∞ is the ambient temperature, ρ_∞ is the air density at ambient temperature, c_p is the specific heat at constant pressure, and g is the gravity acceleration. The non-dimensional form of the critical velocity changes is shown in Fig. 3 using Eqs. 5 and 6.

As shown in this figure the developed method accurately predicts the changes in the critical velocity due to the changing in HRR comparing with the benchmark data.

The maximum gas temperature beneath the ceiling is another appropriate parameter to validate the developed method. According to the theoretical and experimental studies, the maximum gas temperature difference between the ceiling and the ambient (ΔT_{max}) is proportional to:

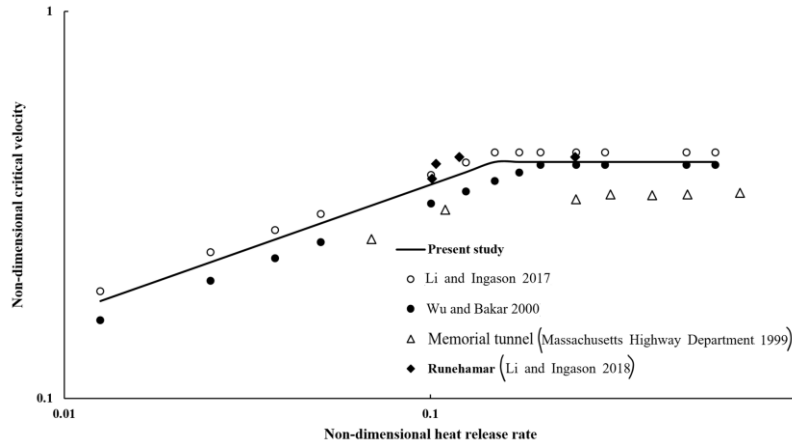


Fig. 3. Developed method validation in terms of the critical velocity.

$$\Delta T_{\max} \approx \frac{HRR}{V_{inlet} b_f^{1/3} H_{eff}^{5/3}} \quad (7)$$

Where in this equation HRR, V_{inlet} , b_f , and H_{eff} are heat release rate of fire, inlet velocity of the tunnel, fire source length scale, and effective height of the tunnel, respectively. The effective height of the tunnel is the vertical distance between the fire source and the ceiling. The above equation is valid for the inlet velocities higher than 19% of the plume characteristic velocity (w^*), which is calculated as:

$$w^* = \frac{HRR_c \times g}{(\rho_0 c_p T_0 b_f)^{1/3}} \quad (8)$$

In this equation HRR_c is the convective heat release rate, which is equal to 70% of the heat release rate in the radiation fraction model. Also, g , ρ_0 , c_p , and T_0 are gravity acceleration, ambient density, specific heat at constant pressure, and ambient temperature, respectively. In order to validate the present method, the changes of ΔT_{\max} are correlated

by $\frac{HRR}{V_{inlet} b_f^{1/3} H_{eff}^{5/3}}$ and shown in Fig. 4.

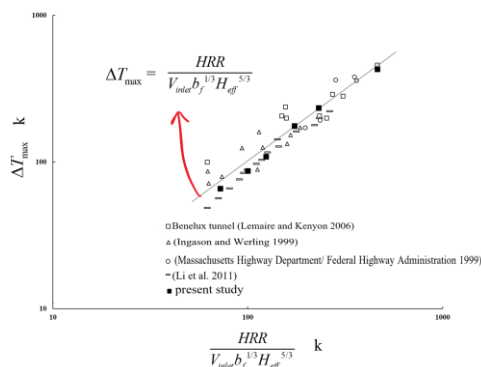


Fig. 4. Developed method validation in terms of the maximum gas temperature beneath the ceiling.

In this figure, the benchmark data are collected from the real tunnels, e.g. memorial tunnel (Massachusetts Highway Department/ Federal

Highway Administration 1999), Benelux tunnel (Lemaire and Kenyon 2006), the experimental measurements of Ingason and Werling (Ingason and Werling 1999), and the experimental study of Li *et al.* (2011). As shown in this figure the developed method could predict accurately the maximum temperature of fire-induced buoyant gases beneath the ceiling.

Furthermore, to more validate the present method the local temperature variation in the tunnel fire situations is verified here. The experimental benchmark data of Hu *et al.* (Hu *et al.* 2007) is used to verify the numerical results. The benchmark data is measured at the full-scale tunnel (88m long, 8m wide, and 2.65m high) for the two different fire sizes of 0.75MW and 1.6MW. The detailed information about the experimental verification setup was presented in the benchmark study (Hu *et al.* 2007). The validation results are shown in Fig. 5. As shown in this figure, the developed method predicts accurately the temperature distribution of the fire-induced hot flow beneath the tunnel ceiling.

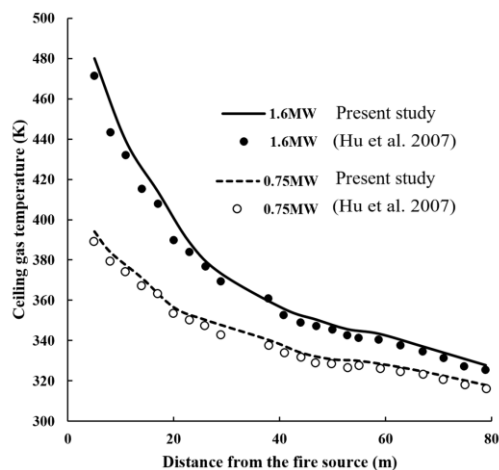


Fig. 5. Developed method validation by verifying the local temperature distribution for two different fire sizes.

According to Fig. 3, Fig. 4, and Fig. 5 the developed method can accurately predict the smoke

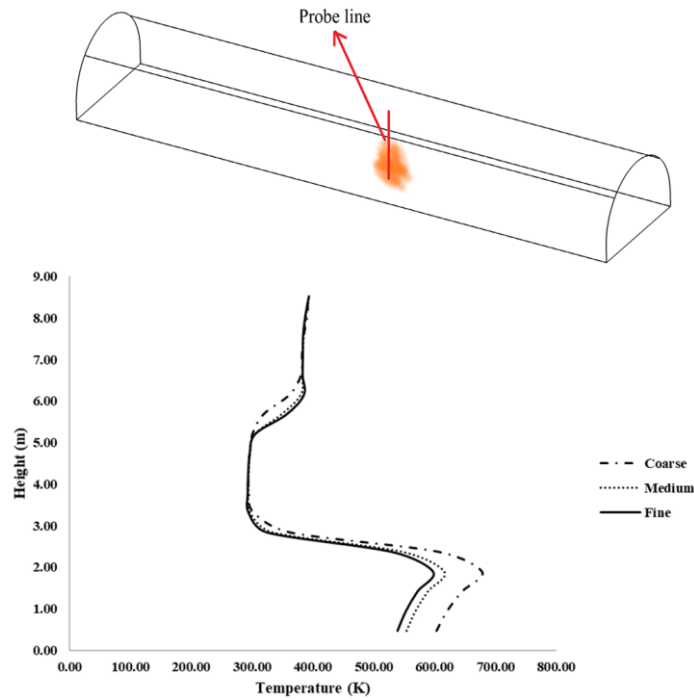


Fig. 6. Grid independence study at the flame region.

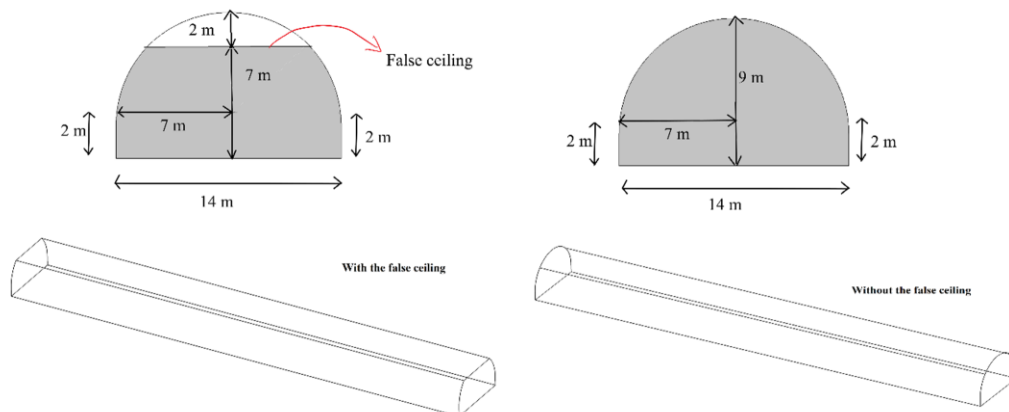


Fig. 7. Geometries investigated to study the effects of the use of the false-ceiling.

flow characteristics, e.g. the critical velocity, which is the minimum inlet velocity required to stop the smoke from the backlayering, and the maximum gas temperature beneath the ceiling.

In all of the performed numerical test runs, the grid sizes in all directions near the fire source were small enough that the meshing was able to cover the flame length scale (Eq. 8) by at least 6-10 computational cells as stated in the literature (Jiang *et al.* 2018; Kazempour *et al.* 2017; McCaffrey 1983; Savalanpour *et al.* 2019):

$$L_f = \left[\frac{HRR}{\rho_\infty T_\infty C_p \sqrt{g}} \right]^{2/5} \quad (9)$$

In this equation L_f is the flame height, T_∞ is the ambient absolute temperature (K), ρ_∞ is the air

density at ambient temperature, c_p is the specific heat at constant pressure, and g is the gravity acceleration.

As an example of the grid independence studies, the temperature profiles of the 3 different grid size categories are compared on the 1D vertical probe line at the center of the fire source for 20MW fire power and 2m/s inlet velocity of the Tohid tunnel without the false-ceiling. The grid sizes (Δy) are normalized using the flame height (Eq.9) as $\frac{\Delta y}{L_f}$. The

coarse, medium and fine grid categories represent $\frac{\Delta y}{L_f}$ values of 3, 6, and 10. The results of the grid independence study are shown in Fig.6.

As shown in this figure, the results would be grid-independent at the non-dimensional grid sizes of 6 to 10.

3. SOLUTION OF THE PROBLEM

In order to investigate the effects of the use of false-ceiling on smoke flow control, two different tunnels with and without the false-ceiling are considered as shown in Fig. 7.

To generalize the results, the non-dimensional analysis is done in the present study using the hydraulic height of the tunnels as the characteristic length in the dimensional analysis. In order to take into account the effect of the presence of false-ceiling, the hydraulic height of the tunnel with false-ceiling is assumed to be equal to the tunnel hydraulic height without the false-ceiling, which is a reasonable assumption, because the false-ceiling is an extension to the tunnel geometry. The cross-sectional hydraulic heights (four times the flow area divided by the wetted perimeter) of the tunnel with and without the false-ceiling are 9.4m and 10.5m, respectively, while we used 10.5 as the characteristic length in the dimensional analysis. The critical velocity and the maximum gas temperature beneath the ceiling are studied to determine the magnitude of the effect of false-ceiling. The boundary condition of the constant velocity (at the tunnel inlet) and the boundary condition of the constant (zero) pressure (at the tunnel outlet) are used in the 3D simulations. The walls and the ceiling of the tunnels are adiabatic boundaries.

Also, the size of the fire source (a cube-shaped, with equal height, width, and length) is selected according to the flame characteristic length calculated in Eq. 9, for all of the numerical test runs.

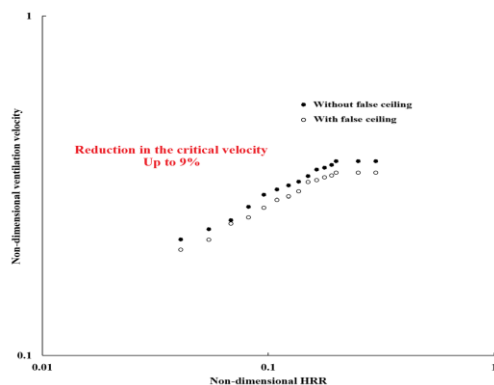


Fig. 8. Effects of the false-ceiling in terms of the critical velocity.

3.1 Critical Velocity

The non-dimensional critical velocity changes of the tunnels with and without the false-ceiling due to the changes in the non-dimensional HRR are shown in Fig. 8. A wide range of the fire HRRs (3MW to 120MW, corresponding to the non-dimensional HRRs of 0.01 to 0.3) and a common range of the ventilation velocities (1m/s to 4m/s) are used in the simulations to find the critical velocities of each of HRRs (shown in Fig. 8). As can be seen, the critical

velocity becomes independent of HRR at the non-dimensional HRRs greater than 0.2 (Wu and Bakar 2000).

As shown in this figure, the critical velocity of the tunnel with the false-ceiling is significantly smaller (up to 9%) than the typical tunnel (without the false-ceiling). In order to more clarify the effects of false-ceiling and to provide an example of the 3D simulation results, a sample test run with 20 MW fire power (0.05 non-dimensional HRR) and 2 m/s inlet air velocity (0.197 non-dimensional inlet velocity) is chosen from the set of performed test runs. Here, the temperature contours and isosurfaces (>400K) are shown in Fig. 9 and Fig. 10, respectively.

According to Fig. 9 and Fig. 10 the backlayering length of the fire-induced hot buoyant gases is reduced. The backlayering length reduction represents the smaller required inlet velocity to stop the smoke from moving toward the tunnel inlet, so the critical velocity will be reduced.

In order to clarify the causes of the differences between the results of the tunnel with and without the false-ceiling, Figure 11 shows the temperature contours at the cross-sections near the fire source (at the collision point of the buoyant plume and the ceiling).

As shown in the above figure the ceiling airflow moves toward the top edges of the flat ceiling and then comes down along the vertical wall of the tunnel. The right and left sides of the flat ceiling are far enough from the fire source and its blockage, so the airflow escapes from the wings of the cross-section toward the outlet. On the other hand, in the circular cross-section (without the false-ceiling), the ceiling hot flow comes smoothly down the curved wall and fill the thicker layer than the square cross-section, so there is not enough space for hot flow to escape from the cross-section wings and the ventilation system of the full circle tunnel should increase the ventilation velocity to overcome the smoke backlayering. Therefore, the critical velocity and the backlayering length of the curved cross-sectional tunnels are higher than the rectangular tunnels.

The hydraulic heights of the Tohid tunnel without and with the false-ceiling are different, so the dimensional analysis should be performed to broaden the applicability of the results. Therefore, in order to generalize the results and establish the effect of the false-ceiling on the smoke backlayering length, a series of scenarios are taken into account in the non-dimensional form (to eliminate the effects of the tunnel sizes) by using various non-dimensional HRR including 0.01, 0.05, 0.1, and 0.2, which correspond to the tunnel fire sizes of 3MW to 80MW (calculated by Eq.6). The variation of the backlayering length is depicted in Fig. 12 for the different fire sizes. As shown in this figure, the backlayering length reduces as the ventilation velocity increases. Also, the zero backlayering length corresponds to the critical velocity. In other words, the critical velocities can be calculated by

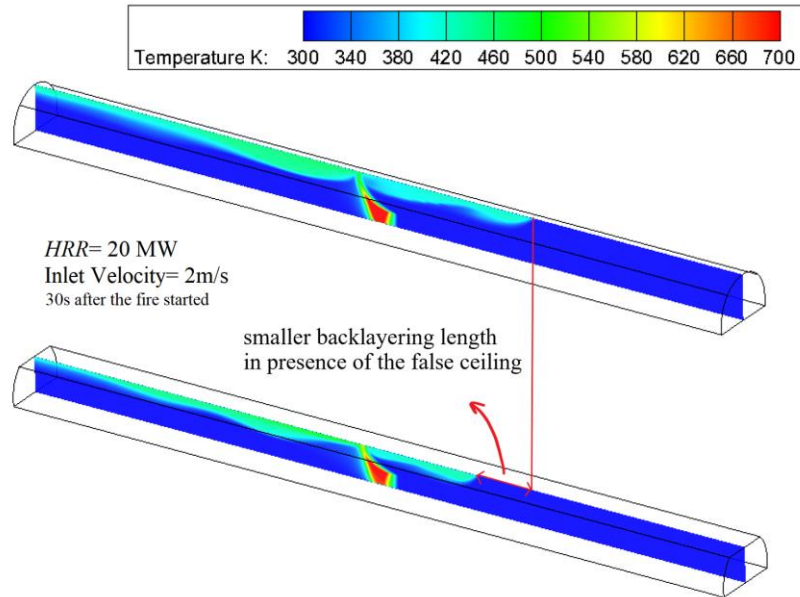


Fig. 9. Effects of the false-ceiling in terms of the temperature contours.

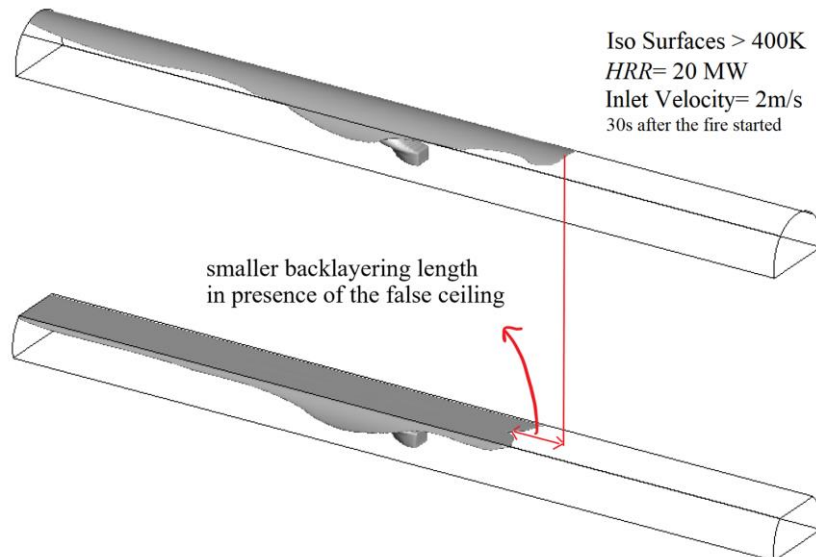


Fig. 10. Effects of the false-ceiling in terms of the temperature isosurfaces(>400K).

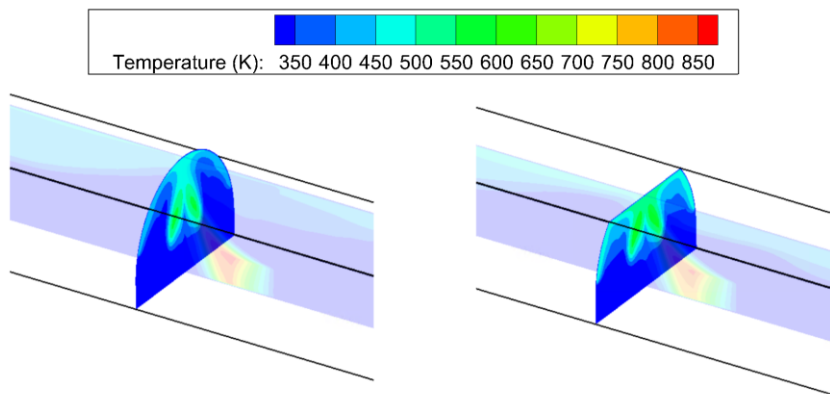


Fig. 11. Temperature distribution of the tunnels with and without the false-ceiling.

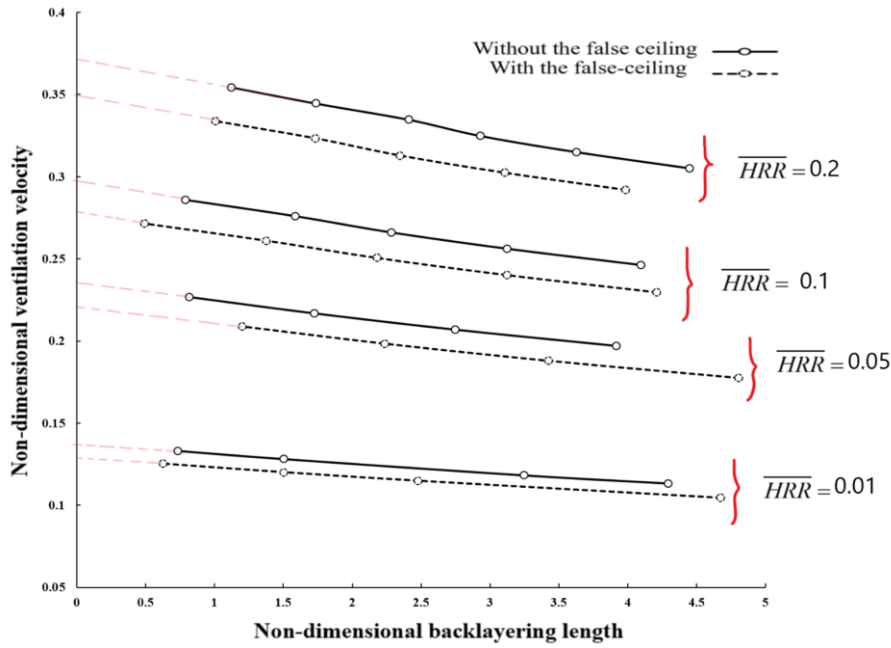


Fig. 12. Effects of the false-ceiling in terms of the non-dimensional backlayering length.

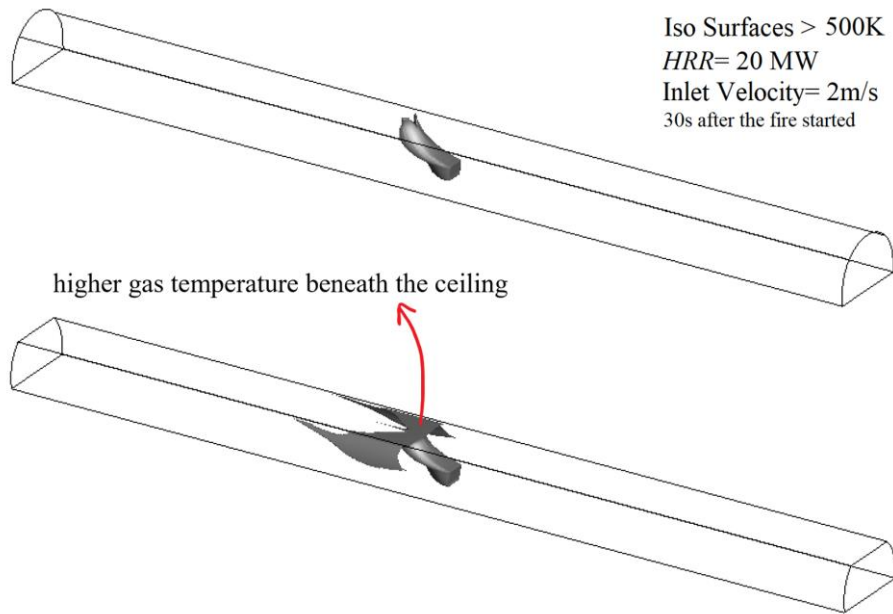


Fig. 13. Effects of the false-ceiling in terms of the temperature isosurfaces (>500K).

extrapolating the results. The non-dimensional ventilation velocity \bar{V}_{inlet} and non-dimensional backlayering length $\bar{L}_{backlayering}$ are calculated as:

$$\bar{V}_{inlet} = \frac{V_{inlet}}{\sqrt{gH}} \quad (10)$$

$$\bar{L}_{backlayering} = \frac{L_{backlayering}}{H} \quad (11)$$

According to this figure, the backlayering lengths of the Tohid tunnel with the false-ceiling are smaller than the Tohid tunnel without the false-ceiling for

all of the non-dimensional HRRs. Also, the critical velocities of the Tohid tunnel with the false-ceiling, extrapolated from the results shown in this figure, are smaller than the Tohid tunnel without the false-ceiling for all of the investigated non-dimensional HRRs.

3.2 Maximum Gas Temperature Beneath the Ceiling

In order to investigate the effects of the use of false-ceiling in terms of the ceiling gas temperature and to provide an example of the simulation results, a sample test run with 20 MW fire power (0.05 non-

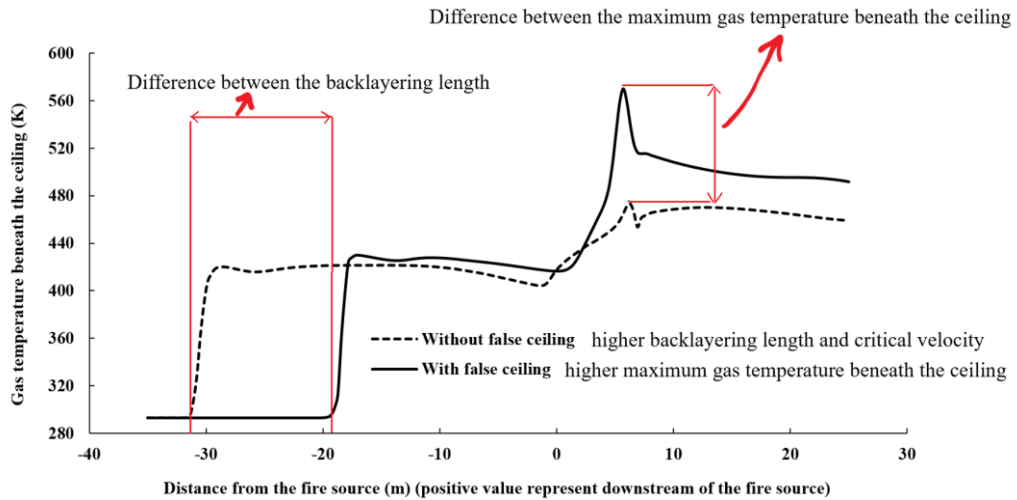


Fig. 14. Fire-induced gas temperature beneath the ceiling for the tunnels with and without the false-ceiling.

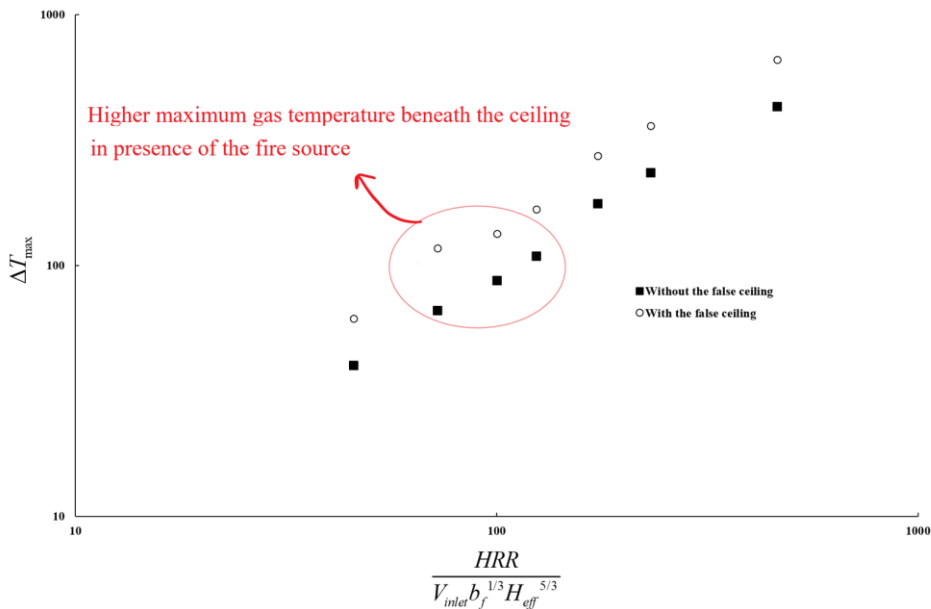


Fig. 15. Effects of the false-ceiling in terms of the maximum gas temperature difference beneath the ceiling.

dimensional HRR) and 2 m/s inlet air velocity (0.197 non-dimensional inlet velocity), is chosen from the set of performed test runs. The temperature isosurfaces greater than 500 K are shown in Fig. 13.

According to Fig. 13, the hot region beneath the ceiling is wider for the tunnel with the false-ceiling than for the tunnel without the false-ceiling. Also, the use of false-ceiling increases the maximum gas temperature beneath the ceiling. The increase in the maximum ceiling gas temperature is mainly because the false-ceiling reduces the vertical difference between the ceiling and the fire source. According to the analytical relation presented in Eq.7, the maximum ceiling gas temperature increases as the vertical difference between the ceiling and the fire source decreases. In other words, a constant heat release rate has a greater

effect on the lower ceiling tunnels. As stated above, the false-ceiling reduces the critical velocity and smoke backlayering length and increases the maximum gas temperature beneath the ceiling, as illustrated in Fig. 14. This figure shows the 1D gas temperature profiles beneath the ceiling for the tunnels with and without the false-ceiling, 30 s after a 20 MW fire started in presence of the inlet velocity of 2 m/s.

As shown in this figure the backlayering length is reduced from 30 m to 20 m, while the maximum gas temperature beneath the ceiling is increased from 473 K to 570 K.

As stated, the hydraulic heights of the Tohid tunnel without and with the false-ceiling are different, so the dimensional analysis should be performed to broaden the applicability of the results. Therefore,

in order to generalize the results, the effects of the use of false-ceiling in terms of the maximum gas temperature beneath the ceiling are investigated in the following form (explained as follows) to eliminate the effects of the tunnel sizes. For this purpose, Fig. 15 shows the maximum gas temperature difference (with respect to ambient temperature) beneath the ceiling for the different sets of fire characteristics, e.g. HRR, fire source length scale, inlet velocity, and effective height, integrated into .

As shown in this figure, the use of false-ceiling results in the increase of the maximum gas temperature beneath the ceiling.

This is mainly because, at the constant hydraulic height (the characteristic length for the dimensional analysis), the effective height (distance from the fire source to the ceiling) is smaller for the tunnel with the false-ceiling. Therefore, according to Eq.7, the temperature difference increases using the false-ceiling.

4. CONCLUSION

In the present study, the effect of the use of false-ceiling was investigated using a 3D developed finite volume CFD (computational fluid dynamics) method. The developed method was validated by comparing the non-dimensional results in terms of the critical velocity and the maximum gas temperature beneath the ceiling with the benchmark data. In order to study the effects of the use of false-ceiling, the detailed results of the tunnels with the false-ceiling including the changing trends of the critical velocity, smoke backlayering length, and the maximum ceiling gas temperature, and the corresponding 3D temperature contours, isosurfaces, and 1D temperature profiles are compared to the similar results of the tunnels with the false-ceiling. According to the results, the use of false-ceiling reduces the smoke backlayering length and the critical velocity, while increases the maximum gas temperature beneath the ceiling. The numerical results had been dimensionless using the dimensional analysis to generalize the presented results and interpretations.

REFERENCES

Al Hadad, W., D. Maillet and Y. Jannot (2018) Experimental transfer functions identification: Thermal impedance and transmittance in a channel heated by an upstream unsteady volumetric heat source. *International Journal of Heat and Mass Transfer* 116, 931-939.

Hu, L. H., N. K. Fong, L. Z. Yang, W. K. Chow, Y. Z. Li and R. Huo (2007) Modeling fire-induced smoke spread and carbon monoxide transportation in a long channel: Fire Dynamics Simulator comparisons with measured data. *Journal of Hazardous Materials* 140(1), 293-298.

Ingason, H. and P. Werling (1999) *Experimental*

study of smoke evacuation in a model tunnel, FOA Defence Research Establishment.

Ingason, H., Y. Z. Li and A. Lönnemark (2014) *Tunnel Fire Dynamics*. Springer, New York.

Jiang, L., M. Creyssels, A. Mos and P. Salizzoni (2018) Critical velocity in ventilated tunnels in the case of fire plumes and densimetric plumes. *Fire Safety Journal* 101, 53-62.

Kazemipour, A., A. Afshin and B. Farhanieh (2017) Numerical-Analytical Assessment of Fire and Ventilation Interaction in Longitudinally Ventilated Tunnels Using Jet Fans. *Heat Transfer Engineering* 38(5), 523-537.

Kazemipour, A., M. Pourghasemi, H. Afshin and B. Farhanieh (2016) Investigation of Fire Growth and Spread in a Model-Scale Railcar Using an Applied Approach. *Journal of Applied Fluid Mechanics* 9(1), 279-292.

Lemaire, T. and Y. Kenyon (2006) Large Scale Fire Tests in the Second Benelux Tunnel. *Fire Technology* 42(4), 329-350.

Li, Y. Z. and H. Ingason (2012) The maximum ceiling gas temperature in a large tunnel fire. *Fire Safety Journal* 48, 38-48.

Li, Y. Z. and H. Ingason (2017) Effect of cross section on critical velocity in longitudinally ventilated tunnel fires. *Fire Safety Journal* 91, 303-311.

Li, Y. Z. and H. Ingason (2018) Discussions on critical velocity and critical Froude number for smoke control in tunnels with longitudinal ventilation. *Fire Safety Journal* 99, 22-26.

Li, Y. Z., B. Lei and H. Ingason (2011) The maximum temperature of buoyancy-driven smoke flow beneath the ceiling in tunnel fires. *Fire Safety Journal* 46(4), 204-210.

Lou, B., Y. Qiu and X. Long (2017) Maximum Smoke Temperature in Non-Smoke Model Evacuation Region for Semi-Transverse Tunnel Fire. *Journal of Applied Fluid Mechanics* 10(4), 1139-1151.

Massachusetts Highway Department/ Federal Highway Administration (1999) Memorial Tunnel Fire Test Ventilation Program, Commonwealth of Massachusetts, Central Artery/Tunnel Project.

Mc Caffrey, B. J. (1983) Momentum implications for buoyant diffusion flames. *Combust Flame* 52, 149-167.

Mc Dermott, R. (2009) FDS Wall Flows Part I: Straight Channels.

Salehi, M. S., M. Askarishahi and S. Radl (2017) Analytical solution for thermal transport in packed beds with volumetric heat source. *Chem Eng J* 316, 131-136.

Savalanpour, H., B. Farhanieh and H. Afshin (2019) Numerical simulation to investigate the induced buoyant flow characteristics caused

- by intensive heat in complex curvilinear geometries. *Heat Tran Asian Res* 48(3), 835-853.
- Wang, F., M. Wang, R. Carvel and Y. Wang (2017) Numerical study on fire smoke movement and control in curved road tunnels. *Tunn Undergr Sp Tech* 67, 1-7.
- Wu, Y. and M. A. Bakar (2000) Control of smoke flow in tunnel fires using longitudinal ventilation systems—a study of the critical velocity. *Fire Saf J* 35(4), 363-390.
- Zhang, S., H. Yang, Y. Yao, K. Zhu, Y. Zhou and X. Cheng (2017) Numerical Investigation of Back-Layering Length and Critical Velocity in Curved Subway Tunnels with Different Turning Radius. *Fire Technol* 53(5), 1765-1793.